Doping- and pressure-induced change of electrical and magnetic properties in the Fe-based spin-ladder compound $BaFe_2Se_3$

Fei Du,[1,2] Yasuyuki Hirata,[1] Kazuyuki Matsubayashi,[1,3] Yoshiya Uwatoko,[1,3] Yutaka Ueda,[1,3] and Kenya Ohgushi[1,3,4]

[1]*Insititute for Solid State Physics, University of Tokyo, Kashiwanoha, Kashiwa, Chiba 277-8581, Japan*

[2]*Key Laboratory of Physics and Technology for Advanced Batteries (Ministry of Education), College of Physics, Jilin University, Changchun 130012, People's Republic of China*

[3]*JST, TRIP, 5 Sanbancho, Chiyoda, Tokyo 102-0075, Japan*

[4]*Department of Physics, Tohoku University, Sendai, Miyagi 980-8578, Japan*

(Received 1 June 2014; revised manuscript received 25 July 2014; published 27 August 2014)

We have investigated the evolution of electronic structure in the Fe-based ladder compound $Ba(Fe_{1-x}Co_x)_2Se_3$ ($0 \leqslant x \leqslant 0.15$) by means of resistivity, magnetic susceptibility, and reflectivity measurements. Although the Co substitution into $BaFe_2Se_3$ greatly decreases the resistivity, the compound still shows an insulating behavior at $x = 0.15$. Moreover, the insulating state at $x = 0.15$ is robust even under the high pressure of 8 GPa. The antiferromagnetic transition temperatures are gradually suppressed by substituting Co atoms at $x \leqslant 0.10$, while the spin glass state is observed at $x \geqslant 0.125$. Our finding revealed that the substituted Co atoms play a dual effect: electron-carrier dopant and localized moment, providing a supplemental insight into the doping effect in the Fe-based superconductors.

DOI: 10.1103/PhysRevB.90.085143 PACS number(s): 74.70.Xa, 74.62.Fj, 75.30.Cr, 75.10.Pq

I. INTRODUCTION

Motivated by the discovery of Fe-based high-temperature superconductivity (SC), the studies on Fe-based pnictides and chalcogenides have aroused remarkable interest [1,2]. Although many new compounds exhibiting SC with high-transition temperature (T_c) have been found, complete comprehension of the mechanism of SC is still unclear and controversial. Considering the crystal structure of the Fe-based superconductors found so far, all the compounds have two-dimensional conducting planes composed of a square lattice of Fe atoms coordinated tetrahedrally by pnictogens or chalcogens [2]. Although there is no finding of SC in Fe-based compounds with one- or three-dimensional structures, elucidating the electronic states of those compounds is expected to give an important clue to the mechanism of SC as well as a strong hint in the search for new superconducting materials.

Recently, AFe_2Se_3 [3–11] (A = K, Cs, and Ba), a series of quasi-one-dimensional spin-ladder compounds, have attracted much attention due to their similar structural motif as those of Fe-based superconductors. In the crystal structure of $BaFe_2Se_3$ (space group, orthorhombic *Pnma*), Fe^{2+} ions are coordinated tetrahedrally by Se^{2-} ligand ions, and each $FeSe_4$ tetrahedron is connected to another by sharing edges, forming a Fe ladder extending along the b axis (the inset of Fig. 1). Though a superconducting transition at $T_c = 11$ K is found for $BaFe_2Se_3$ in an earlier study [3], later reports [4–7] confirmed the Mott insulator with a charge gap of 0.2 eV. The compound undergoes an antiferromagnetic (AFM) transition at 240–256 K [3–5,7]. The magnetic structure is revealed to be block type: four Fe spins form a ferromagnetic cluster and the cluster aligns antiferromagnetically with another [5]. Importantly, the magnetic moment is much reduced from the theoretically expected high-spin value $4\mu_B$ to $2.75\mu_B$, possibly because the compound is in the vicinity of the metal-insulator transition boundary. An interesting question is the carrier-doping effect in this compound. If one can successfully introduce mobile carriers as in the case of two-dimensional Fe-based superconductors, one can possibly metallize the system and render the system superconducting. However, this cannot be easily achieved, since the strong electron correlation effect is prominent in a one-dimensional structure, making the carriers localized. Indeed, the hole-doped system $Ba_{1-x}K_xFe_2Se_3$ exhibits insulating behaviors at any x values. Here, we employ the Co substitution for $BaFe_2Se_3$ to investigate the electronic structure of the electron-doped ladder compound. Our systematic study on the transport, magnetic, and optical properties reveals that the substituted Co atoms have a dual nature: electron-carrier dopant and localized moment.

II. EXPERMENT

Single crystalline $Ba(Fe_{1-x}Co_x)_2Se_3$ ($0 \leqslant x \leqslant 0.15$) was synthesized by the slow-cooling method. Small Ba chunks, Fe powders, Co powders, and Se powders were mixed together according to the stoichiometric ratio Ba:Fe:Co:Se = $1:2(1-x):2x:3$. The mixture was then placed into a carbon crucible, and the crucible was sealed in a quartz tube under 0.3 atm of Ar atmosphere. The quartz tube was heated at 1150 °C for 40 h and slowly cooled to 750 °C at approximately 6 °C/h. The black crystal was obtained with a typical size of $5\times2\times1$ mm^3. The crystals were characterized by x-ray diffraction at room temperature using SmartLab and R-AXIS RAPID II diffractometers (Rigaku), where Cu $K\alpha$ and Mo $K\alpha$ radiations are used, respectively. The chemical composition of the obtained crystals was determined to be the same as the nominal composition within an experimental accuracy of $\Delta x = \pm0.02$ by energy-dispersive x-ray spectroscopy (EDX). The critical doping level turned out to be $x = 0.15$, above which some impurity phases emerge.

The electrical resistivity was then measured by the standard four-probe method at ambient and high-pressure conditions; in the latter case, hydrostatic pressure was generated by a cubic anvil cell immersed in a cryostat [12]. The magnetic susceptibility was measured by a superconducting quantum

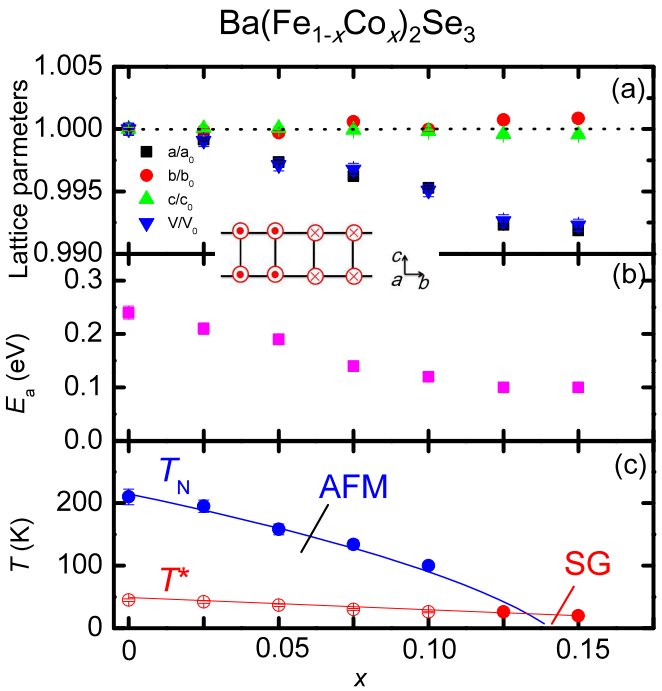

FIG. 1. (Color online) The doping dependence of the lattice parameters and volume (a), the obtained activation energy (E_a) deduced from the resistivity in the temperature region between 230 and 300 K (b), and the magnetic transition temperature (T_N and T^*) (c) for $Ba(Fe_{1-x}Co_x)_2Se_3$ ($0 \leqslant x \leqslant 0.15$). The inset shows the block-type magnetic structure for $BaFe_2Se_3$. AFM and SG in (c) stand for the antiferromagnetic and spin glass states, respectively.

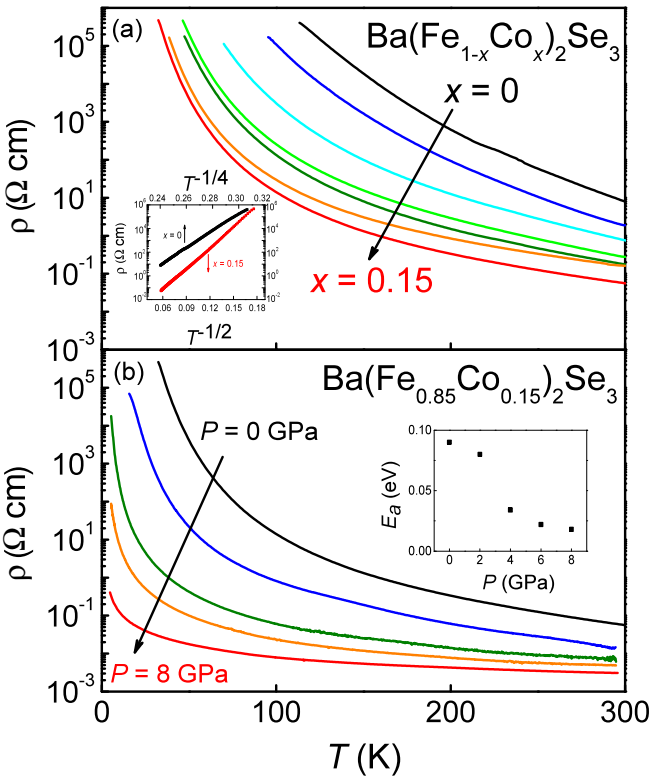

FIG. 2. (Color online) Temperature (T) dependence of resistivity (ρ) along the ladder direction for $Ba(Fe_{1-x}Co_x)_2Se_3$ with $x = 0$, 0.025, 0.05, 0.075, 0.10, 0.125, and 0.15 under ambient pressure (a) and the same data for $Ba(Fe_{0.85}Co_{0.15})_2Se_3$ under the pressure (P) of 0, 2, 4, 6, and 8 GPa (b). The inset of (a) shows the fitting results to the variable-range-hopping model. The inset of (b) shows the pressure dependence of the calculated activation energy (E_a).

interference device magnetometer (Quantum Design). Polarized reflectivity spectra were measured for the *bc* surface polished with Al_2O_3 powders. A Fourier-transform infrared spectrometer and a grating spectrometer were used for measurements in the energy range of 0.1–0.9 and 0.7–4.3 eV, respectively. Optical conductivity spectra were obtained from the reflectivity spectra by the Kramers-Kronig transformation.

III. RESULTS

Figure 1(a) shows a relative change of unit-cell parameters and volume determined via the powder x-ray diffraction patterns taken for the ground single crystals of $Ba(Fe_{1-x}Co_x)_2Se_3$. There is a clear decrease in the a value perpendicular to the two-leg ladder plane. On the other hand, the b value along the leg direction and the c value along the rung direction slightly depend on the x value. These lattice parameter changes are reminiscent of Co-substituted $BaFe_2As_2$ [13,14], in which a large lattice shrinkage perpendicular to the FeAs plane with increasing Co content is observed. The volume shrinkage on substituting Co atoms is more consistent with the smaller ionic radius of Co^{2+} ions (0.58 Å) than with Fe^{2+} ions (0.63 Å) [15]. Note that despite the changes of lattice parameter on the Co doping, the space group of $Ba(Fe_{1-x}Co_x)_2Se_3$ remains unchanged and belongs to the orthorhombic *Pnma* as confirmed by our single crystal x-ray diffraction measurements (data not shown).

The temperature (T) dependence of the resistivity (ρ) along the leg direction for $Ba(Fe_{1-x}Co_x)_2Se_3$ ($0 \leqslant x \leqslant 0.15$) is shown in Fig. 2(a). All the samples investigated here are insulators in the measured T regime. On Co substitution, the resistivity at 300 K decreases from 7.8 Ω cm at $x = 0$ to 0.06 Ω cm at $x = 0.15$, indicating that the system becomes closer to a metallic state. Indeed, the charge gap (E_a) estimated by the fitting of ρ between 230 and 300 K with the thermal-activation-type equation is suppressed from 0.24 eV at $x = 0$ to 0.09 eV at $x = 0.15$, as shown in Fig. 1(b). In contrast to the activation behavior at the high T regime, ρ at the low T regime is well described by the variable-range-hopping (VRH) model $\rho \propto \exp[(\Delta/T)^{1/(1+d)}]$, where Δ and d donate the characteristic energy and the dimension in the VRH model. The dimension characterizing the conducting behavior gradually changes from $d = 3$ at $x = 0$ to $d = 1$ at $x = 0.15$, as shown in the inset of Fig. 2(a); the mechanism of this crossover phenomenon is not clear at present.

In order to survey the possible metallization, we performed high-pressure resistivity measurements for a selected sample $x = 0.15$. As shown in Fig. 2(b), upon application of pressure, ρ gradually decreases, and the ρ value under 8 GPa at 300 and 50 K is almost one and five orders of magnitude smaller than the ρ value under ambient pressure, respectively. However, no metallic state is observed. The ρ at $230 \leqslant T \leqslant 300$ K

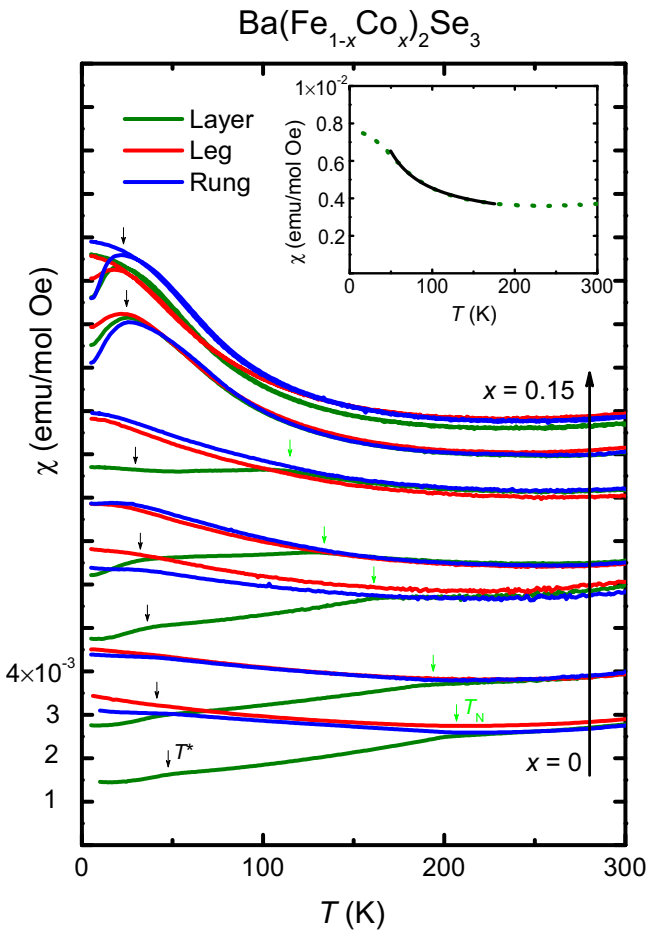

FIG. 3. (Color online) Temperature (T) dependence of the magnetic susceptibility (χ) for $Ba(Fe_{1-x}Co_x)_2Se_3$ with $x = 0$, 0.025, 0.05, 0.075, 0.10, 0.125, and 0.15. The magnetic field of 5 T is applied to the three principal axes: a, b, and c axes correspond to the layer, leg, and rung directions, respectively. The data taken at the zero-field-cooled condition are shown; in addition, for $x = 0.15$, the data taken in both the zero-field-cooled and field-cooled conditions are shown. The arrows indicate the magnetic transition at T_N and T^*. Note that each curve is shifted by 1×10^{-3} emu/mol Oe for clarity. The inset shows the Curie-Weiss fitting between 50 and 175 K for χ along the a axis at $x = 0.15$.

can be well fitted with the thermal-activation-type equation, and the obtained activation energy is plotted in the inset of Fig. 2(b). These results indicate that the localization of the doped electrons is quite robust in the present system.

Figure 3 shows the T dependence of the magnetic susceptibility (χ) measured under a magnetic field of 5 T applied along the three principal axes for $Ba(Fe_{1-x}Co_x)_2Se_3$. The susceptibility for $x = 0$ shows a nearly linear decrease with decreasing T at the high T regime, which is in stark contrast to the conventional Curie-Weiss behavior in Mott insulators. This abnormal decrease of χ on cooling is also discernible in the paramagnetic state of $BaFe_2As_2$ (Ref. [16]) and LaFeAsO (Ref. [17]), and is likely related to the evolution of an antiferromagnetic correlation. Indeed, strong antiferromagnetic fluctuations are observed by the powder neutron diffraction in the paramagnetic state of $BaFe_2Se_3$ (Ref. [5]). Another striking feature is that χ at $x = 0$ displays a strong anisotropy below $T_N = 210$ K; this corresponds to the long-range AFM ordering. T_N is slightly lower than the reported values 240, 255, and 256 K, probably due to the undetectable Fe deficiencies in the EDX analysis [3–5,7]. A faster drop of χ along the a axis indicates that the a axis is the easy axis, consistent with the previous neutron scattering studies [5,9]. On further cooling, the χ curve shows an additional anomaly at around $T^* = 45$ K; such an anomaly, though also reported in the earlier susceptibility study [4], is not observed in the powder neutron diffraction profiles [5,7]. At present, the origin of this anomaly remains unclear; however, we speculate that the magnetocrystalline anisotropy is more pronounced below T^* for a certain reason.

When Co atoms are substituted into the Fe site, T_N decreases gradually. A further increase of Co contents results in the disappearance of AFM ordering at $x = 0.125$. We also note that the difference between the χ value along the layer direction and the χ value along the other two directions at the lowest T measured is greatly suppressed on the Co substitution, which is likely related to the reduced magnetocrystalline anisotropy. On the contrary, the T^* transition is quite robust against the Co substitution, and persists up to $x = 0.15$. Hence, a magnetic phase without commensurate magnetic order appears as the ground state at $x = 0.15$. Since there is a difference in the χ curves taken in the field-cooled and zero-field-cooled conditions below T^* at $x = 0.15$, we identify the low-temperature phase as the spin glass or cluster glass state. One possible mechanism of the formation of this glassy state is that the increase of the magnetic anisotropy below T^* bears anisotropic spins, which easily freeze into the glassy state.

The χ curve in the paramagnetic state continues to decrease on cooling at the low x range; however, it turns from a gradual decrease on cooling at the high T regime to a gradual increase on cooling at the low T regime (typically below 100 K) at the high x range. The gradual increase in χ at the low T regime becomes more distinct with increasing x, and this phenomenon is most likely due to the formation of localized moments of the Co^{2+} ions. To estimate the effective moments of Co^{2+} ions, we fit χ along the a axis for $x = 0.15$ between 50 and 175 K with the modified Curie-Weiss law $\chi = \chi_0 + \frac{C}{T}$, as shown in the inset of Fig. 3. χ_0 and C are obtained to be 0.0026(1) emu/mol and 0.200(4) emu K/mol, respectively. If we assume that χ_0 and Curie-Weiss terms represent contributions from Fe and Co atoms, respectively, we can deduce the effective moment of Co^{2+} spins to be $\mu_{eff} = 2.30\mu_B$, which is slightly larger than the theoretical value of the low-spin state of Co^{2+} ions ($\mu_{eff} = 1.73\mu_B$).

Reflectivity and optical conductivity spectra with the light polarization along the leg direction for $x = 0$ and 0.15 are shown in Figs. 4(a) and 4(b), respectively. In the optical conductivity spectrum of $x = 0$ at room temperature, one can see two Mott-like excitation modes at the energy $E = 0.6$ and 1.7 eV; the absorption edge of the low-energy mode is close to twice the activation energy determined from the resistivity, 0.2 eV. In comparison with it, in the spectrum of $x = 0.15$ at room temperature, the mode at $E = 1.7$ eV is slightly weakened, and the low-energy tail structure shows up in the 0.6 eV mode. On cooling the $x = 0.15$ sample, a dip feature appears at 0.4 eV and one can recognize a new excitation mode at 0.2 eV

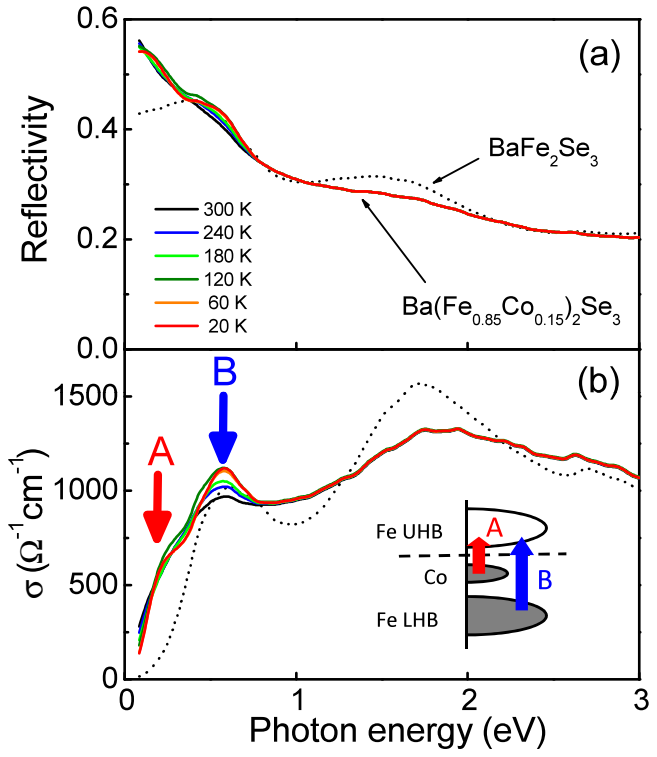

FIG. 4. (Color online) Reflectivity (a) and optical conductivity (σ) spectra (b) as a function of photon energy for $BaFe_2Se_3$ (broken lines) and $Ba(Fe_{0.85}Co_{0.15})_2Se_3$ (solid lines). The modes *A* and *B* correspond to an excitation from in-gap states, and a Mott excitation, respectively. The inset of (a) depicts the band structure involved with the low-energy optical excitations. LH and UH indicate the lower and upper Hubbard bands of Fe 3*d* electrons.

[labeled by *A* in Fig. 4(b)]. This 0.2 eV mode corresponds to the excitation related to the electron carriers introduced by the Co substitution. The formation of such in-gap states indicates that the electrons are successfully doped into a band composed of Fe and Co *d* orbitals by the Co substitution; however, they are localized around Co atoms, keeping the system an insulator.

IV. DISCUSSION

Now, we discuss the phase diagram of $Ba(Fe_{1-x}Co_x)_2Se_3$ by comparing it with those of $Ba(Fe_{1-x}Co_x)_2As_2$ and $La_{2-x}Sr_xCuO_4$, which are prototypical Fe-based and cuprate superconductors, respectively. (1) The parent compound $BaFe_2Se_3$ is a Mott insulator with a small charge gap; therefore, in terms of the electron correlation effect, the compound is located in between the correlated metal $BaFe_2As_2$ and the Mott insulator with large charge gap La_2CuO_4. (2) The magnetic structure of $BaFe_2Se_3$ as a block type differs from the stripe type in $BaFe_2As_2$ and the checkerboard type in La_2CuO_4. The block-type magnetism in $BaFe_2Se_3$ is hardly explained by the weak-coupling nesting instability as in $BaFe_2As_2$ and the strong-coupling superexchange interaction as in La_2CuO_4. Previous reports [5–7] revealed that the block-type AFM ordering of $BaFe_2Se_3$ is driven by the large lattice distortion, hinting at the importance of orbital degrees of freedom. (3) The charge gap of $Ba(Fe_{1-x}Co_x)_2Se_3$ gradually decreases with increasing x; however, the metallic state never appears at any x value in contrast to the metallic state achieved in $Ba(Fe_{1-x}Co_x)_2As_2$ and $La_{2-x}Sr_xCuO_4$, which might be explained by the localized electrons in the one-dimensional structure compared with the two-dimensional structure. (4) The T_N is suppressed with increasing x in $Ba(Fe_{1-x}Co_x)_2Se_3$ as in the cases of $Ba(Fe_{1-x}Co_x)_2As_2$ and $La_{2-x}Sr_xCuO_4$. However, the critical concentration x_c, where the antiferromagnetic long-range order is fully destroyed, differs in between: $x_c \sim 0.125$ in $Ba(Fe_{1-x}Co_x)_2Se_3$, $x_c \sim 0.038$ in $Ba(Fe_{1-x}Co_x)_2As_2$ (Ref. [18]), and $x_c \sim 0.02$ in $La_{2-x}Sr_xCuO_4$ (Ref. [19]). The largest x_c in $Ba(Fe_{1-x}Co_x)_2Se_3$ could be caused by an insulating nature of the system; mobile electrons can easily destroy the long-range AFM ordering. (5) The spin glass state appears after the long-range magnetic order has been destroyed in $Ba(Fe_{1-x}Co_x)_2Se_3$, contrasting with the direct transition from the antiferromagnetic and superconducting states in $Ba(Fe_{1-x}Co_x)_2As_2$. Instead, the appearance of the spin glass state resembles the phase diagram of $La_{2-x}Sr_xCuO_4$ (Ref. [20]). One interpretation of these features is that the disorder effect on the magnetism is much more pronounced in the Mott insulating state on the verge of Mott transition.

Up to now, we have simply assumed that electrons are doped by the Co substitution; however, we should recall a great controversy on the substituting effect of transition-metal atoms such as Co, Ni, and Cu in Fe-based superconductors [21–25]. Wadati *et al.* proposed a localization model in which the extra electrons of the transition metal are fully localized within the muffin-tin sphere of the substituted site and hardly affect the Fermi surface [21]. This claim apparently contradicted many observations that the Fermi surface volume estimated by angle-resolved photoemission spectroscopy (ARPES) as well as the effective carrier number estimated by the Hall coefficient measurements evolves as itinerant electrons are doped by the chemical potential shift [26–28]. The latest first-principles calculations narrow the gap between theory and experiment by revealing that the Co substitution results in the emergence of incoherent carriers accompanied by the loss of coherent spectral weight; this means the existence of both localized and itinerant carriers [22]. This dual nature of doped electrons is confirmed by the detailed ARPES experiments for $Ba(Fe_{1-x}M_x)_2As_2$ (M = Co, Ni, and Cu), which demonstrate that the extra electron number estimated from the Fermi surface volume is smaller than the nominal value depending on the depth of the impurity potentials of the substituted transition metal [23].

Even though our study on $Ba(Fe_{1-x}Co_x)_2Se_3$ is not yet extended to ARPES measurements, the dual role of the substituted Co atoms manifests itself through a close inspection of the resistivity and magnetic susceptibility data. At the low x region ($0 \leqslant x \leqslant 0.1$), the substituted Co atoms mainly play the role of carrier dopant. This is indicated by the fact that the resistivity decreases greatly and the activation energy shows an obvious decrease with increasing x, which can be well understood as the carrier density increase by the Co substitution. Moreover, the AFM ordering is suppressed by the Co substitution, further evidence of the substituted Co atoms serving the mobile electron carriers to the system. If the Co^{2+} spins are fully localized keeping the electronic configurations of each Fe^{2+} ion the same as in the parent compounds, T_N is not as sensitive to the x value as in the case of Zn-substituted

La_2CuO_4 (Refs. [29,30]). On the other hand, the substituted Co atoms also behave as the localized moment at the high x region ($0.1 \leqslant x \leqslant 0.15$). This can be seen from the weakened tendency of resistivity decrease and the nearly same activation energy between $x = 0.125$ and 0.15. More importantly, in these compositions, there appears a tendency to a gradual increase in χ at the low T regime as the manifestation of the localized moments. The localized moments are considered to freeze below T^* at $x = 0.15$, exhibiting the spin glass transition.

Finally, we briefly discuss the reasons why the Fe-based ladder compound $Ba(Fe_{1-x}Co_x)_2Se_3$ is hardly metallized. As discussed above, electrons are successfully incorporated into the Fe $3d$ bands by the Co substitution and are responsible for the conduction at the low x region. Simultaneously, the antiferromagnetic order becomes unstable. However, at the high x region, the doped electrons are more easily trapped around the substituted Co atoms due to the strong impurity potential. In other words, the random potential introduced by the site disorder between the Fe^{2+} and Co^{2+} ions is so strong that the electrons are localized according to the Mott-Anderson localization mechanism. This localization of carriers prevents the further decrease of resistivity and disables the metallization. Considering these electronic states, we can propose several methods to metallize $BaFe_2Se_3$. One is the use of carrier doping by replacing Ba and Se sites, since the chemical substitution into these sites does not bear a large disorder in the electronic structure. Since the hole-doped system $Ba_{1-x}K_xFe_2Se_3$ (Ref. [9]) has been proved to be an insulator, it is better to try the electron doping. Another useful method is to increase the dimensionality by applying pressure. Not only uniaxial pressure but also hydrostatic pressure is known to modify the effective dimensionality of the electronic system, since the lattice is compressed in an anisotropic manner in the one-dimensional system. If one can widen the bandwidth by increasing the dimensionality, the electrons can be delocalized and possibly form Cooper pairs. The applied pressure of 8 GPa in our measurements is not enough, therefore experiments in much higher pressure are highly expected.

V. CONCLUSION

We report the resistivity, magnetic susceptibility, and reflectivity spectra for the single crystals of $Ba(Fe_{1-x}Co_x)_2Se_3$ ($0 \leqslant x \leqslant 0.15$). We found a successive decrease of resistivity with the Co substitution, keeping an insulating behavior. The antiferromagnetic transition temperature decreases gradually, and the antiferromagnetic long-range order is fully suppressed at $x = 0.125$. At $x = 0.15$, the spin glass state was found to be the ground state. We discussed the dual role of the substituted Co atoms: the electron dopant and the localized moment. The site disorder introduced by the Co substitution and the smaller bandwidth in the one-dimensional structure prevent the metallization of this spin-ladder system.

ACKNOWLEDGMENT

This research was supported by the Grant Program of the Yamada Science Foundation.

[1] Y. Kamihara, T. Watanabe, M. Hirano, and H. Hosono, J. Am. Chem. Soc. **130**, 3296 (2008).
[2] G. R. Stewart, Rev. Mod. Phys. **83**, 1589 (2011).
[3] A. Krzton-Maziopa, E. Pomjakushina, V. Pomjakushin, D. Sheptyakov, D. Chernyshov, V. Svitlyk, and K. Conder, J. Phys.: Condens. Matter **23**, 402201 (2011).
[4] H. C. Lei, H. Ryu, Anatoly I. Frenkel, and C. Petrovic, Phys. Rev. B **84**, 214511 (2011).
[5] Y. Nambu, K. Ohgushi, S. Suzuki, F. Du, M. Avdeev, Y. Uwatoko, K. Munakata, H. Fukazawa, S. X. Chi, Y. Ueda, and T. J. Sato, Phys. Rev. B **85**, 064413 (2012).
[6] B. Saparov, S. Calder, B. Sipos, H. B. Cao, S. X. Chi, David J. Singh, Andrew D. Christianson, Mark D. Lumsden, and Athena S. Sefat, Phys. Rev. B **84**, 245132 (2011).
[7] J. M. Caron, J. R. Neilson, D. C. Miller, A. Llobet, and T. M. McQueen, Phys. Rev. B **84**, 180409(R) (2011).
[8] F. Du, K. Ohgushi, Y. Nambu, T. Kawakami, M. Avdeev, Y. Hirata, Y. Watanabe, T. J. Sato, and Y. Ueda, Phys. Rev. B **85**, 214436 (2012).
[9] J. M. Caron, J. R. Neilson, D. C. Miller, K. Arpino, A. Llobet, and T. M. McQueen, Phys. Rev. B **85**, 180405(R) (2012).
[10] E. Dagotto, Rev. Mod. Phys. **85**, 849 (2013).
[11] Q. L. Luo, A. Nicholson, J. Rincón, S. H. Liang, J. Riera, G. Alvarez, L. M. Wang, W. Ku, G. D. Samolyuk, A. Moreo, and E. Dagotto, Phys. Rev. B **87**, 024404 (2013).
[12] K. Igawa, H. Okada, H. Takahashi, S. Matsuishi, Y. Kamihara, M. Hirano, H. Hosono, K. Matsubayashi, and Y. Uwatoko, J. Phys. Soc. Jpn. **78**, 025001 (2009).
[13] K. Park, D. Louca, A. Llobet, and J. Q. Yan, Phys. Rev. B **84**, 024512 (2011).
[14] N. Ni, M. E. Tillman, J. Q. Yan, A. Kracher, S. T. Hannahs, S. L. Bud'ko, and P. C. Canfield, Phys. Rev. B **78**, 214515 (2008).
[15] R. D. Shannon, Acta Crystallogr., Sect. A: Found. Crystallogr. **32**, 751 (1976).
[16] X. F. Wang, T. Wu, G. Wu, H. Chen, Y. L. Xie, J. J. Ying, Y. J. Yan, R. H. Liu, and X. H. Chen, Phys. Rev. Lett. **102**, 117005 (2009).
[17] R. Klingeler, N. Leps, I. Hellmann, A. Popa, U. Stockert, C. Hess, V. Kataev, H.-J. Grafe, F. Hammerath, G. Lang, S. Wurmehl, G. Behr, L. Harnagea, S. Singh, and B. Büchner, Phys. Rev. B **81**, 024506 (2010).
[18] P. C. Canfield, S. L. Bud'ko, N. Ni, J. Q. Yan, and A. Kracher, Phys. Rev. B **80**, 060501 (2009).
[19] M. A. Kastner, R. J. Birgeneau, G. Shirane, and Y. Endoh, Rev. Mod. Phys. **70**, 897 (1998).
[20] J. Chang, Ch. Niedermayer, R. Gilardi, N. B. Christensen, H. M. Rønnow, D. F. McMorrow, M. Ay, J. Stahn, O. Sobolev, A. Hiess, S. Pailhes, C. Baines, N. Momono, M. Oda, M. Ido, and J. Mesot, Phys. Rev. B **78**, 104525 (2008).
[21] H. Wadati, I. Elfimov, and G. A. Sawatzky, Phys. Rev. Lett. **105**, 157004 (2010).
[22] T. Berlijn, C. H. Lin, W. Garber, and W. Ku, Phys. Rev. Lett. **108**, 207003 (2012).
[23] S. Ideta, T. Yoshida, I. Nishi, A. Fujimori, Y. Kotani, K. Ono, Y. Nakashima, S. Yamaichi, T. Sasagawa, M. Nakajima, K. Kihou, Y. Tomioka, C. H. Lee, A. Iyo, H. Eisaki, T. Ito, S. Uchida, and R. Arita, Phys. Rev. Lett. **110**, 107007 (2013).

[24] T. Berlijn, P. J. Hirschfeld, and W. Ku, Phys. Rev. Lett. **109**, 147003 (2012).

[25] G. Levy, R. Sutarto, D. Chevrier, T. Regier, R. Blyth, J. Geck, S. Wurmehl, L. Harnagea, H. Wadati, T. Mizokawa, I. S. Elfimov, A. Damascelli, and G. A. Sawatzky, Phys. Rev. Lett. **109**, 077001 (2012).

[26] V. Brouet, M. Marsi, B. Mansart, A. Nicolaou, A. Taleb-Ibrahimi, P. Le Fèvre, F. Bertran, F. Rullier-Albenque, A. Forget, and D. Colson, Phys. Rev. B **80**, 165115 (2009).

[27] F. Rullier-Albenque, D. Colson, A. Forget, and H. Alloul, Phys. Rev. Lett. **103**, 057001 (2009).

[28] N. Katayama, Y. Kiuchi, Y. Matsushita, and K. Ohgushi, J. Phys. Soc. Jpn. **78**, 123702 (2009).

[29] S. T. Ting, P. Pernambuco-Wise, J. E. Crow, E. Manousakis, and J. Weaver, Phys. Rev. B **46**, 11772 (1992).

[30] T. Machi, I. Kato, R. Hareyama, N. Watanabe, Y. Itoh, N. Koshizuka, S. Arai, and M. Murakami, Physica C **388–389**, 233 (2003).